Proton array focused by a laser-irradiated mesh

Zhai, S. H., Shen, B. F., Borghesi, M., Wang, W. P., Zhang, H., Kar, S., Ahmed, H., Li, J. F., Li, S. S., Wang, C., Lu, X. M., Wang, X. L., Xu, R. J., Yu, L. H., Leng, Y. X., Liang, X. Y., Li, R. X., & Xu, Z. Z. (2019). Proton array focused by a laser-irradiated mesh. *Applied Physics Letters*, *114*(1), Article 013509. Advance online publication. https://doi.org/10.1063/1.5054884

Published in:
Applied Physics Letters

Document Version:
Peer reviewed version

Proton Array Focused by a Laser-irradiated Mesh

S.H.Zhai[1,2,3], B.F.Shen[1,4*], M. Borghesi[3], W.P.Wang[1†], H.Zhang[1‡], S.Kar[3], H.Ahmed[3], J.F.Li[1], S.S.Li[1,2], H.Zhang[1,2], C.Wang[1], X.M.Lu[1], X.L.Wang[1,2], R.J.Xu[1], L.H.Yu[1] , Y.X.Leng[1], X.Y.Liang[1], R.X.Li[1] and Z.Z.Xu[1]

[1] State Key Laboratory of High Field Laser Physics, Shanghai Institute of Optics and Mechanics, Chinese Academy of Sciences, Shanghai 201800, China

[2]University of Chinese Academy of Sciences, Beijing 100049, China

[3]Centre for Plasma Physics, The Queen's University of Belfast, BT71NN Belfast, UK

[4]Department of Physics, Shanghai Normal University, Shanghai 200234, China

We present a technique on focusing laser-driven proton beams in an array pattern by employing a copper mesh irradiated by a separate, intense laser pulse. Transient fields are generated on the mesh following the intense interaction. Under the combined effect of collisional scattering and electrical deflections from the mesh, a laser-driven proton beam is split into multiple focused beams with high density of ~4×10^9/cm^2 after propagation through the charged-up mesh. The particle density within the focused beamlets is up to ~11 times the initial density of the proton beam. Multiple beams focusing through this approach may open routes for proton beam conditioning, leading to opportunities for multi-beam applications, such as tomographic radiography and proton implantation.

Intense laser pulses can be used to generate high brightness proton beams with energies of multi mega-electron-volts [1, 2]. These energetic proton beams have potential applications in medical therapy [3-5] and radiobiology [6, 7], proton radiography [8-10] high-energy-density physics [11], space electronics testing [12] and inertial confinement fusion [13]. Recently, MeV proton with kHz repetition rate is obtained in experiment [14]. In most cases, target normal sheath acceleration [15, 16] (TNSA) is chosen as a feasible mechanism to generate energetic protons for laser intensity on scale of 10^{19}-10^{20} W/cm^2 and target thickness on scale of microns. However, the inherent characteristics of the TNSA regime, such as the large divergence with which proton flux decreases fast with distance and broad exponential energy spectrum [17], limit its direct applications.

Several different methods have led to breakthroughs in divergence reduction for proton beams. Controlling transient electromagnetic fields in a target through laser-plasma interactions is now an established approach for focusing and energy selection of proton beams [18-21]. An alternative method for divergence control is by employing specially curved targets [22-25], for ballistic focusing of the particles. In addition, magnets and solenoid coils have also been applied for beam shaping and energy selection [26-28]. All the above-mentioned methods have been applied to focus the whole proton beam, or a portion, concentrating the particles within a single spot. In this letter, we present an approach, which, with the help of transient fields generated on a mesh target, allows obtaining an array of multiple beam foci with the same arrangement as the

mesh structure.

A focused proton array, similar to the light beams focused by a lens array, is composed of multiple proton-beams with high density. Providing a series of separate beamlets may be useful for the development of approaches to tomographic radiography employing laser-driven protons (e.g. combining target shaping to the multifoci approach described here). Additionally, it may be of interest to ion implantation techniques for the processing of arrayed structures, such as in semiconductor device fabrication [29]. Compared with full-beam focusing, multiple beams improve the efficiency in proton utilization and leads to faster operations in ion implantation.

The experiments here reported were carried out in the State Key Laboratory of High Field Laser Physics in China. FIG. 1 shows the set-up of the experiment for proton-array focusing with a copper mesh. After amplification and compression, a 0.8-μm laser pulse is split into two separate pulses CPA1 and CPA2 by a semi-transparent mirror with a split ratio of 7:3, where CPA1 and CPA2 respectively takes 70% and 30% energy of the laser beam. For proton generation, CPA1 with a duration of ~50 fs and energy of 12.3 J was focused onto a 4-μm thick Al foil at an incident angle of ~12° to the target normal. The focal spot shown in FIG. 1(b) was ~13 μm full-width at half maximum (FWHM) which encompasses 40% energy of the laser pulse (~4J), corresponding to an intensity of $\sim 7\times10^{19}$ W/cm^2. The contrast ratio of CPA1 is around 10^{-8}. A second ~5.2J laser beam (CPA2) was focused onto the center of a grounded Cu mesh whose radius

is ~40 μm with an intensity of ~2.1×10^{18} W/cm^2. The mesh thickness is 30 μm while the period (in the *y*-*z* plane) is 100 μm including a 70-μm gap and a 30-μm wide bar. The laser's incidence angle is 40° to the normal to the mesh target. The distance from the Al foil to the copper mesh was l = 5 mm. For proton detection, a stack of radio-chromic film (RCF) was placed at a distance of L = 45 mm from the mesh, corresponding to a magnification of 10 (calculated as $(L+l)/l = 10$). The RCF stack was shielded with a 15-μm Al foil to prevent plasma or x-ray contamination of the first layers.

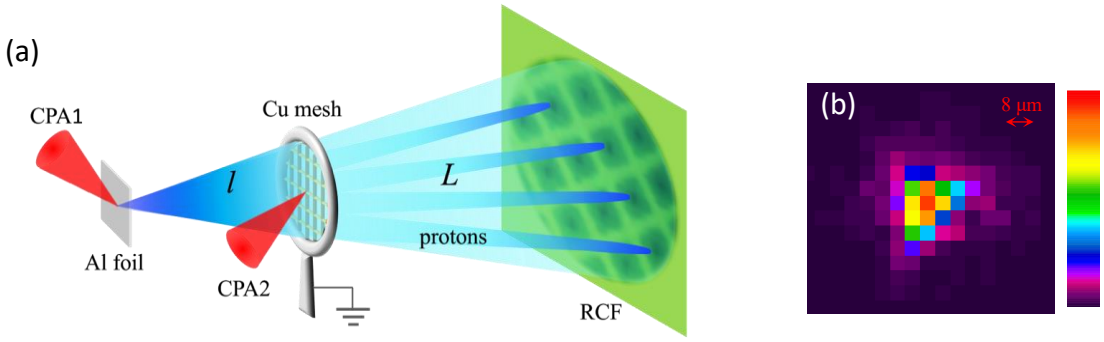

FIG. 1 (a) Schematic representation of the setup for the generation of a focused proton array. CPA1 irradiates onto the Al foil for proton generation while CPA2 irradiates a Cu mesh for transient fields generation. A proton beam generated from the rear surface of the Al foil is divided into several beamlets and a focusing effect for each beamlet arises from the electric fields on the mesh wires. The transmitted proton beamlets are detected by RCF. (b) Focusing spot of CPA1 detected by CCD with the resolution of 4 μm.

Protons passing through the bars of the copper mesh are scattered away from their initial trajectories due to elastic collisions within the bars. As a result, the beam is divided into several beamlets and a shadow of the mesh structure is recorded on the RCF [30]. Furthermore, strong, transient fields will be generated on the mesh [31-33], owing to the irradiation of CPA2 and the expulsion of

relativistic electrons from the mesh wires [34]. If the protons (generated from the rear surface of the Al foil) reach the mesh target while these fields are present, they are also acted upon by the fields, in addition to the collisional effects.

FIG. 2 shows the experimental proton distribution in two representative shots (shot (a) and shot (b)). The red circles at the meshes' center represent the locations of the laser spot. FIGs. 2(a1), (a2) and (a3) show the distribution of protons with energy of 2.9±0.15 MeV, 4.3±0.1 MeV and 5.4±0.1 MeV in shot (a). The protons in FIG .2(a1) appear to be focused, within small dark dots at the centre of the grid squares in some regions of the mesh. A magnified section of the RCF in the red square in FIG. 2(a1) is shown in FIG. 2(c) where the focusing effect of proton beams is clearly visible. No such focusing is observed for the 4.3-MeV protons in FIG. 2(a2) and the 5.4-MeV protons in FIG. 2(a3). The optical delay between the two laser pulses in shot (a) was $\delta l \sim 6.0 \pm 0.1$ cm corresponding to a time delay $\delta t \sim 200.0 \pm 3$ ps and, time of flight of ~2.9-MeV and ~4.3-MeV protons was 212 ps and 175 ps respectively to arrive at the center of the mesh. So it is inferred that the time for CPA2 arriving at the mesh is before the arrival of ~2.9-MeV protons, meaning that these protons can be focused by the transient fields excited by CPA2, while the ~4.3 MeV and higher energy protons, arriving before the interaction, are unaffected. We note that the mesh distortions observed in shot (a) are not caused by the CPA2 irradiation, but arise from poor laminarity in regions of the proton beam, which varies on a shot to shot basis.

For the shot (b) of FIGs. 2(b1), (b2) and (b3), the optical delay between the two CPA pulses was reduced to 167 ±3 ps with reference to the corresponding figures in shot (a) (through shortening the optical path difference between the two laser beams by ~1 cm). Focusing of the 4.3-MeV protons with diagonal streak can now be observed clearly across the mesh (see FIG. 2(b2)). For the whole mesh, the best focusing dots emerge in a range of r~600-700 μm but the focusing effect become worse at further places r ~ 800-900 μm. No clear focusing effect is observed in the irradiation area where we inferred strong field exists when 4.3-MeV protons arrive at the mesh. Protons deposited on other RCF layers are not focused. 4.3-MeV and 2.9-MeV protons with (time of flight ~ 175 ps) arrive now, respectively, ~8 ps and ~45 ps after the CPA2 irradiation. While 5.4 MeV protons are unfocused because they arrive before the CPA2 interaction, the lack of focusing effect for 2.9-MeV protons indicates a significant attenuation of the focusing fields at 45 ps from the irradiation.

FIG. 2(e) shows the size of a tight-focused spot for the 4.3-MeV protons. The diameters of the circles representing relative density of 0.8 and 0.5 with respect to the peak density of ~ 11 n_0 are respectively ~14 μm and ~24 μm, wherein n_0 is the initial density of unfocused beamlets in a grid.

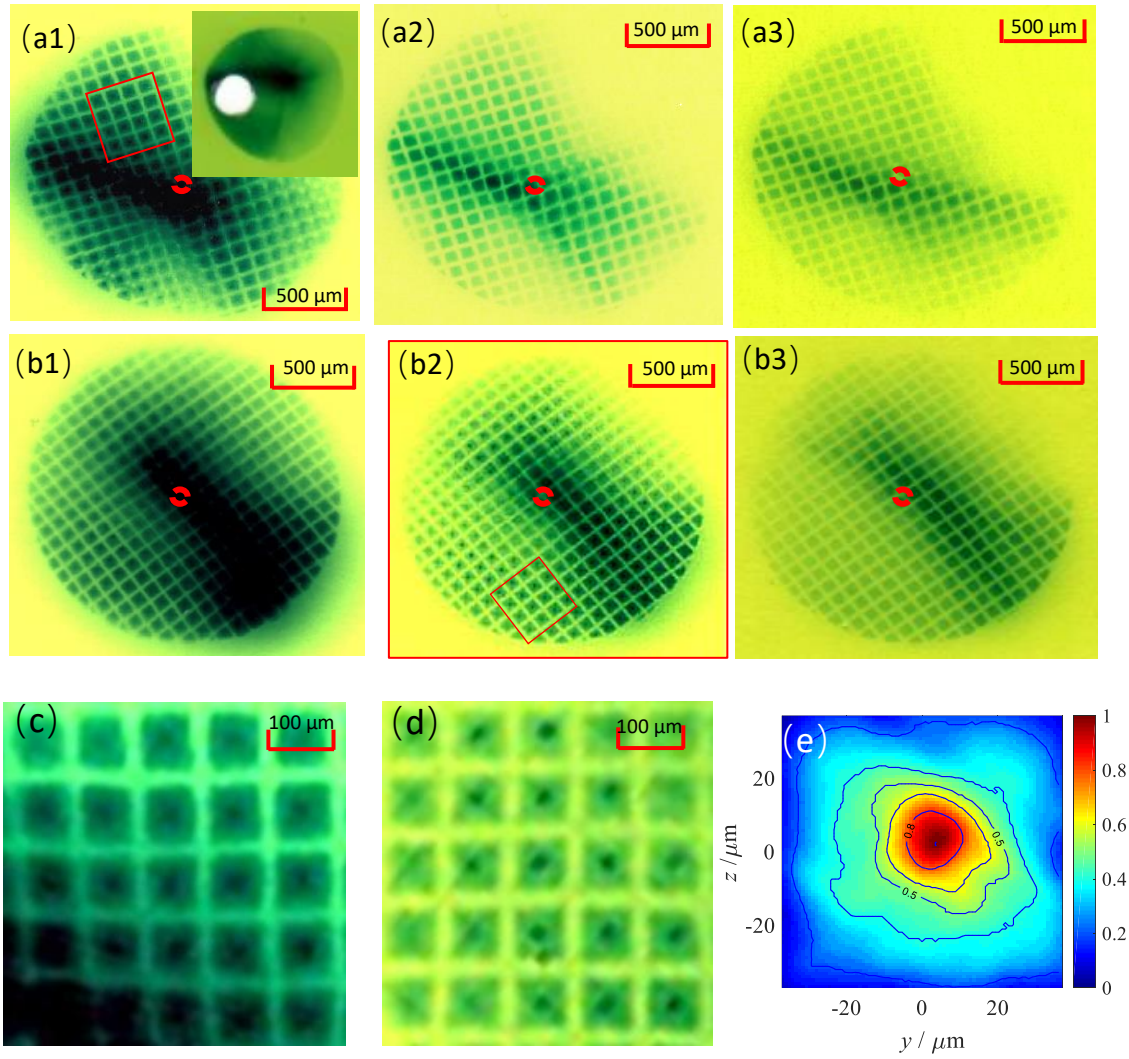

FIG. 2 Distribution of proton beamlets with the energy of (a1) 2.9±0.15-MeV, (a2) 4.3±0.1-MeV and (a3) 5.4±0.1-MeV protons after CPA2 irradiation of the mesh in shot (a) (optical delay between the two pulses equal to δt~200.0 ± 3 ps). The inset in (a1) is the radiography of 2.9-MeV protons without mesh. The hole on the RCF is for energy spectrum detection by TPs. (b1, b2, b3) proton distribution in shot (b) with energy same as in (a1, a2, a3) but for an optical delay of δt~167±3 ps. (c) The magnified part of RCF shown in the red square in FIG. 2(a1). (d) The magnification of the red square shown in FIG. 2(b2). (e) A focused proton beam in a grid.

The general effect observed appears broadly consistent with transient charging of the mesh and the appearance of focusing electric fields for a short period after its irradiation. To learn the details of electromagnetic fields

generation and evolution on the mesh, we ran a 3D simulation with a VSIM code for electromagnetics utilizing a custom-made finite-difference in time-domain (FDTD) algorithm [35]. Different from the PIC simulation with VORPAL code in plasma [36], a mesh target is set as a perfect conductor in the simulation without ionization. Since the emphasis of the simulation is on EM field evolution, plasma dynamics are not considered in the simulation. The mesh target whose radius is 1-mm and connected to ground through a metal wire in $-z$ direction. Same as the experimental situation, the mesh period is 100 μm comprising a 70-μm spacing and a 30-μm wire bar. The simulation area spreads from -0.3 mm to 0.3 mm in x direction, -1.5 mm to 1.5 mm in both y and z directions with 180×780×780 cells. Absorbing boundary condition is set for particles and open condition for EM field.

Hot electrons are initially assumed in a volume of 30 μm ×30 μm ×100 μm connected to the mesh. Based on the parameters of CPA2 pulse, the quantity, temperature and energy spectrum of hot electrons are set. The total number of hot electrons is assumed as $N_{\mathrm{hot}} = \eta E/T_{\mathrm{e}} = 4.6\times10^{13}$, where $\eta = 30\%$ [37] is the energy conversion efficiency from laser to hot electrons, E=5.2 J is the CPA2 energy and T_{e} is the average temperature of the hot electrons expressed as $T_{\mathrm{e}} = \left(\sqrt{1+\frac{a^2}{2}}-1\right)\times 0.511 = 0.14$ MeV with a=1.1 (the normalized laser vector potential). Based on previous estimates for similar irradiation conditions [32,38],

the total number of free electrons, which can escape from the target and positively charge the target is assumed ~ 2× 10^{11} with a spectrum of $dN/dE = (N_{hot}/T_e)e^{-E/Te}$.

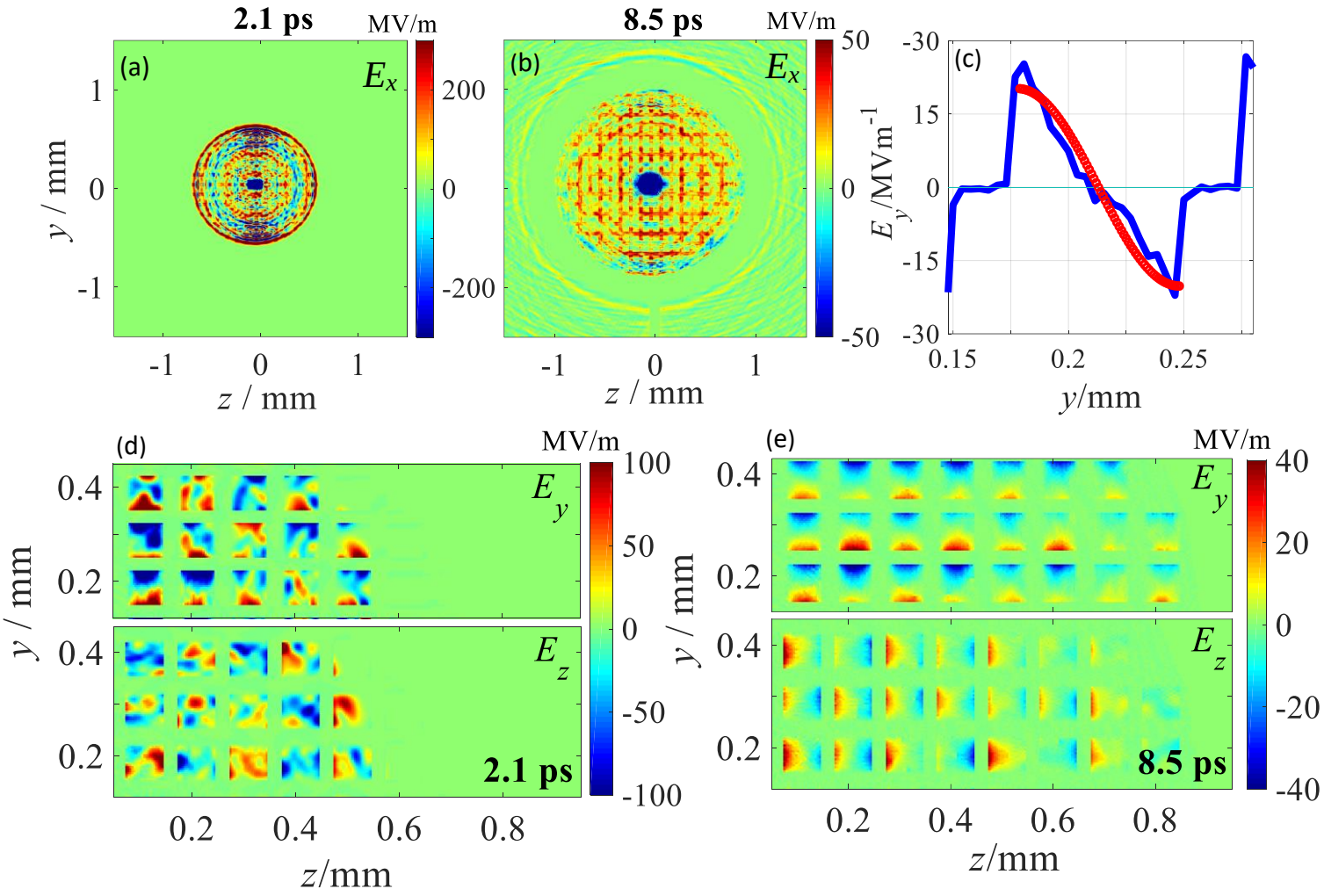

FIG. 3 2D distribution of E_x on the mesh target, (a) at $t1$ = 2.1 ps and (b) $t2$ = 8.5 ps. (c) E_y profile along the y direction across an element of the mesh. The blue line is obtained in VSIM simulation and the red line represents a fit according to the theoretical function discussed in the text. The distribution of E_y and E_z in a small area (d) at $t1$; (e) at $t2$.

The simulation shows that the irradiated area of the mesh target becomes immediately positively charged due to free electrons escape from the irradiated region. The charged region expands outwards at close to the speed of light (e.g.

as observed in [32] and in [39], extending to the whole mesh within 3.5 ps. The propagation of an ultrashort EM pulse is associated to this process as observed in several experiments and simulations [21, 33, 34]. After the charge has spread across the whole mesh, this remains positively charged with a uniform charge density. A quasi-static, regular transverse electric field pattern is formed, which plays a key role for proton focusing.

At $t1$ = 2.1 ps, the charge pulse is in its expanding stage and confined within $r \sim 600$ μm inferred from E_x (the electric field component perpendicular to the plane of the simulation) as shown in FIG. 3(a). At this early stage, the electric field pattern observed in the simulation is complex and irregular (see transverse components E_y and E_z (in FIG. 3(d)) as it will result by the superimposition of radiation field associated to the EM pulse propagation (and associated oscillating currents) and static field from localized net charges. A regular field pattern across the mesh emerges in the simulation only at later times, after the charge pulse has reached the edge of the mesh, and its reflection from the edge has also faded.

For example, at $t2$ = 8.5 ps, it is seen in FIG. 3(b) that positive charge is uniformly distributed on the whole mesh , and a static field pattern is formed on the most part of the whole mesh. Transverse electric field E_z and E_y with an amplitude of several tens of MV/m distributes regularly on the mesh as shown in FIG. 3(e). In a grid element, positive and negative field peaks, with amplitude of order 10^7 V/m are formed at the opposite wires boundary, while the field strength is zero at the grid center as shown in FIG. 3(c). Besides, the field strength is weak.

Such a field pattern will focus protons toward the centre of the grid element and leads to the formation of a diagonal streak of protons.

An analytical approximation of the transverse electric field can be obtained as a combination of trigonometric functions for a closed volume of a grid based on the solution of Laplace equation in a metal square:

$$E_z = -E_0 \Sigma_{mn} \alpha_{mn} \frac{n\pi}{2q} \cos\left(\frac{m\pi}{2q} y\right) \sin\left(\frac{n\pi}{2q} z\right) \exp\left(-\left(\frac{x-100}{30}\right)^2\right),$$

$$E_y = -E_0 \Sigma_{m,n} \alpha_{mn} \frac{m\pi}{2q} \sin\left(\frac{m\pi}{2q} y\right) \cos\left(\frac{n\pi}{2q} z\right) \exp\left(-\left(\frac{x-100}{30}\right)^2\right).$$

We choose a grid fitted with the parameters $m, n = 2, 4, 6$, $q = 175$ μm and $\alpha_{mn} = 0.2, 0.4 \; and \; 1$. The unit of all variables is micron. A one dimensional distribution of E_y along the y direction at $z = 0$ is shown by the red line in FIG. 3(c).

We carried out particle tracing simulations of a 4.3-MeV proton beam, with an initial radius of 20 μm, propagating through the calculated electric field as shown in FIG. 4(a). The lateral velocity of the beam is ignored, since the maximum divergence of each beamlet is 35 μm/5 mm ~ 0.007 rad. We tried electric field with strength of 5.0×10^7 V/m and 1.0×10^8 V/m in separate simulations. The proton distribution at a plane 4.5 cm away from the mesh is shown in FIG. 4(b) and (c). In FIG. 4(b), the maximum focused beam density is more than 3 times the initial density when acted upon by a field strength of 5.0×10^7 V/m. The proton beam is focused at ~23 times the initial density when

acted upon by the field with of 1.0×10^8 V/m shown in FIG. 4(c). For electric field with higher amplitude, such as 10^9 V/m, proton beams will be focused too soon after the mesh and then diverge so that no focusing effect can be obtained at detection plane. Therefore, the focusing field amplitude in experiment must be in the range 5.0×10^7 V/m – 10^8 V/m, which broadly coincides with the VSIM simulation results.

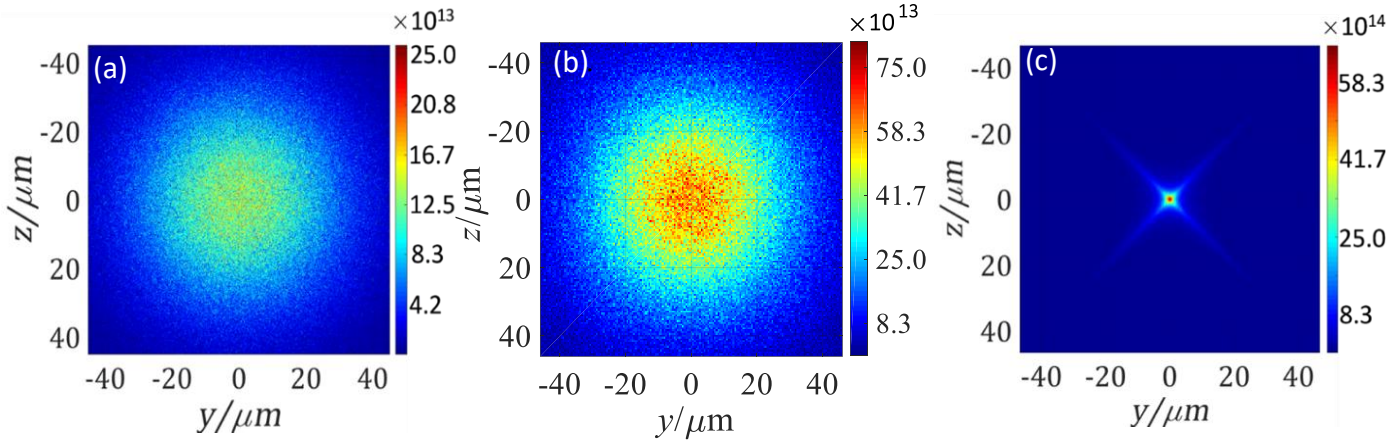

FIG.4 (a) The proton beam initially distributes in Gaussian form with a radius of 20 μm. The distribution of focused proton beam at x = 4.5 cm acted by the electric field with maximum strength of (b) 5×10^7 V/m (c)and 1×10^8 V/m.

In conclusion, we have obtained a focused proton array composed of high-density proton beamlets with the help of a mesh target irradiated by a femtosecond laser pulse. Owing to the irradiation, strong, transient radial electric fields are formed on the mesh. Protons having the right energy to reach the mesh while the fields are active will be focused, which is also verified through simulations. In VSIM simulations, the dynamic process of mesh charging after the irradiation is shown and quasi-static transverse electric fields in a concentric

pattern are generated during the discharging process whose average amplitude is several time 10^7 V/m. We hope that the experimental method will provide a tool for controlling laser-accelerated proton beams and that the focused proton array will help broadening the range of proton applications.

We thank Dr. Longqing Yi and Prof. Liangliang Ji for helpful discussions. This work is funded by the National Nature Science Foundation of China (11335013, 11575274, 11127901 and 11674339), Ministry of Science and Technology of the People's Republic of China (2016YFA0401102, 2018YFA0404803), Strategic Priority Research Program of the Chinese Academy of Sciences (XDB16), Shanghai Natural Science Foundation (Grant No.17ZR1434300) and Engineering and Physical Sciences Research Council (grant EP/K022415/1).

*B.F.Shen (Email: bfshen@mail.shcnc.ac.cn)
†W.P.Wang(Email: wangwenpeng@siom.ac.cn)
‡H.Zhang(Email: zhanghui1989@siom.ac.cn).

[1] E. L. Clark, K. Krushelnick, J. R. Davies, M. Zepf, M. Tatarakis, F. N. Beg, A. Machacek, P. A. Norreys, M. I. K. Santala, I. Watts, et al, *Phys. Rev. Lett*. 84, 670 (2000).

[2] R. A. Snavely, M. H. Key, S. P. Hatchett, T. E. Cowan, M. Roth, T. W. Phillips, M. A. Stoyer, E. A. Henry, T. C. Sangster, M. S. Singh, et al, *Phys. Rev. Lett*. 85, 2945 (2000).

[3] S. Bulanov and V. Khoroshkov, *Plasma Phys. Rep* 28, 453 (2002).

[4] S. V. Bulanov, T. Z. Esirkepov, V. S. Khoroshkov, A. V. Kuznetsov, and F. Pegoraro, *Physics Letters A* 299, 240 (2002).

[5] K. W. D. Ledingham, P. McKenna, T. McCanny, S. Shimizu, J. M. Yang, L. Robson, J. Zweit, J. M. Gillies, J. Bailey, G. N. Chimon, et al, Journal of Physics D: *Applied Physics* 37, 2341 (2004).

[6] S. D. Kraft, C. Richter, K. Zeil, M. Baumann, E. Beyreuther, S. Bock, M. Bussmann, T. E. Cowan, Y. Dammene, W. Enghardt, et al, *New Journal of Physics* 12, 085003 (2010).

[7] J. Bin, K. Allinger, W. Assmann, G. Dollinger, G. A. Drexler, A. A. Friedl, D. Habs, P. Hilz, R. Hoerlein, N. Humble, et al, *Applied Physics Letters* 101, 243701 (2012).

[8] A. J. Mackinnon, P. K. Patel, M. Borghesi, R. C. Clarke, R. R. Freeman, H. Habara, S. P. Hatchett, D. Hey, D. G. Hicks, S. Kar, et al, *Phys. Rev. Lett.* 97, 045001 (2006).

[9] C. A. Cecchetti, M. Borghesi, J. Fuchs, G. Schurtz, S. Kar, A. Macchi, L. Romagnani, P. A. Wilson, P. Antici, R. Jung, et al, *Physics of Plasmas* 16, 43102 (2009).

[10] A. Ravasio, L. Romagnani, S. Le Pape, A. Benuzzi-Mounaix, C. Cecchetti, D. Batani, T. Boehly, M. Borghesi, R. Dezulian, L. Gremillet, et al, *Physical review. E*, Statistical, nonlinear, and soft matter physics 82, 016407 (2010).

[11] G. M. Dyer, A. C. Bernstein, B. I. Cho, J. Osterholz, W. Grigsby, A. Dalton, R. Shepherd, Y. Ping, H. Chen, K. Widmann, et al, *Phys. Rev. Lett.* 101, 015002 (2008).

[12] B Hidding, O Karger, T Königstein, G Pretzler, G G Manahan, P Mckenna, R Gray, R Wilson, S M Wiggins, G H Welsh, et al, *Scientific Reports* (Nature Publisher Group) 7, 42354 (2017).

[13] M. Roth, T. E. Cowan, M. H. Key, S. P. Hatchett, C. Brown, W. Fountain, J. Johnson, D. M. Pennington, R. A. Snavely, S. C. Wilks, et al, *Phys. Rev. Lett.* 86, 436 (2001).

[14] John T Morrison, Scott Feister, Kyle D Frische, Drake R Austin, Gregory K Ngirmang, Neil R Murphy, Chris Orban, Enam A Chowdhury and W M Roquemore, New J. Phys. 20, 069501(2018).

[15] M. Allen, P. K. Patel, A. Mackinnon, D. Price, S. Wilks, and E. Morse, *Phys. Rev. Lett.* 93, 265004 (2004).

[16] S. P. Hatchett, C. G. Brown, T. E. Cowan, E. A. Henry, J. S. Johnson, M. H. Key, J. A. Koch, A. B. Langdon, B. F. Lasinski, R. W. Lee, et al, *Phys. Plasmas* 7,2076 (2000).

[17] S. C. Wilks, A. B. Langdon, T. E. Cowan, M. Roth, M. Singh, S. Hatchett, M. H. Key, D. Pennington, A. MacKinnon, and R. A. Snavely, *Phys. Plasmas* 8, 542 (2001).

[18] O.Willi, T.Tonician, M. Borghesi, J.Fuchs, E. D'Humieres, P.Antici, P.Audebert, E.Brambrink, C.Cecchetti, A.Pipahl and L.Romagnani, *Laser and Particle Beams*. 25, 71-77 (2007).

[19] T. Toncian, M. Borghesi, J. Fuchs, E. d'Humieres, P. Antici, P. Audebert, E. Brambrink, C. A. Cecchetti, A. Pipahl, L. Romagnani, et al, *Science* 312, 410 (2006).

[20] B. Albertazzi, E. d'Humières, L. Lancia, V. Dervieux, P. Antici, J. Böcker, J. Bonlie, J. Breil, B. Cauble, S. N. Chen, et al, *The Review of scientific instruments* 86, 043502 (2015).

[21] Satyabrata Kar, Hamad Ahmed, Rajendra Prasad, Mirela Cerchez, Stephanie Brauckmann, Bastian Aurand, Giada Cantono, Prokopis Hadjisolomou, Ciaran L S Lewis, Andrea Macchi, et al, *Nature Communications* 7, 10792 (2016).

[22] P. K. Patel, A. J. Mackinnon, M. H. Key, T. E. Cowan, M. E. Foord, M. Allen, D. F. Price, H. Ruhl, P. T. Springer, and R. Stephens, *Phys. Rev. Lett.* 91, 125004 (2003).

[23] S. Kar, K. Markey, M. Borghesi, D. C. Carroll, P. McKenna, D. Neely, M. N. Quinn, and M. Zepf, *Phys. Rev. Lett.* 106, 225003 (2011).

[24] T. Bartal, M. E. Foord, C. Bellei, M. H. Key, K. A. Flippo, S. A. Gaillard, D. T. Offermann, P. K. Patel, L. C. Jarrott, D. P. Higginson, et al, *Nature Physics* 8, 139 (2011).

[25] B. Qiao, M. E. Foord, M. S. Wei, R. B. Stephens, M. H. Key, H. McLean, P. K. Patel, and F. N. Beg, *Physical review. E*, Statistical, nonlinear, and soft matter physics 87, 013108 (2013).

[26] M. Schollmeier, S. Becker, M. Geissel, K. A. Flippo, A. Blazevic, S. A. Gaillard, D. C. Gautier, F. Gruner, K. Harres, M. Kimmel, et al, *Phys. Rev. Lett.* 101, 055004 (2008).

[27] K. Harres, I. Alber, A. Tauschwitz, V. Bagnoud, H. Daido, M. Günther, F. Nürnberg, A. Otten, M. Schollmeier, J. Schütrumpf, et al, *Physics of Plasmas* 17, 023107 (2010).

[28] S. Ter-Avetisyan, M. Schnürer, R. Polster, P. V. Nickles, and W. Sandner, *Laser and Particle Beams* 26, 637 (2008).

[29] A Szerling, K Kosiel, M Kozubal, M Myśliwiec, R Jakieła, M Kuc et al, Semicond. Sci. Technol. 31, 075010 (2016).

[30] M. Borghesi, A. J. Mackinnon, D. H. Campbell, D. G. Hicks, S. Kar, P. K. Patel, D. Price, L. Romaganani, A. Schiavi and O. Willi, *Physical Review Letter*, 92, 055003, 2004.

[31] H. Ahmed, S. Kar, G. Cantono, G. Nersisyan, S. Brauckmann, D. Doria, D. Gwynne, A. Macchi, K. Naughton, O. Willi, et al, *Nuclear Instruments and Methods in Physics Research Section A*: Accelerators, Spectrometers, Detectors and Associated Equipment 829, 172 (2016).

[32] M. Borghesi, S. Kar, L. Romagnani, T. Toncian, P. Antici, P. Audebert, E. Brambrink, F. Ceccherini, C. A. Cecchetti, J. Fuchs, et al, *Laser and Particle Beams* 25, 161 (2007).

[33] K. Quinn, P. A. Wilson, C. A. Cecchetti, B. Ramakrishna, L. Romagnani, G. Sarri, L. Lancia, J. Fuchs, A. Pipahl, T. Toncian, et al, *Phys. Rev. Lett*. 102, 194801 (2009).

[34] Shigeki Tokita, Shuji Sakabe, Takeshi Nagashima, Masaki Hashida and Shunsuke Inoue, *Scientific Reports*, 5, 8628, 2015.

[35] VSim, See the online document for the information on electromagnetic and electrostatic simulation with VSim software.

[36] Chet Nieter, John R. Cary, Journal of Computational Physics 196, 448–473 (2004).

[37] R.P.J.Town, C.Chen, L.A.Cottrill, M.H.Key, W.L.Kruer, A.B.Langdon, B.F.Lasinski, R.A.Snavely, C.H.Still, M.Tabak, D.R.Welch, S.C.Wilks, Nucl. Instrum. & Methods A 544, 61 (2005).

[38] J. Dubois, F. Lubrano-Lavaderci, D. Raffestin, J. Ribolzi, J. Gazave, A. Compant La Fontaine, E. d'Humières, S. Hulin, P. Nicolaï, A. Poyé, et al, *Physical review. E*, Statistical, nonlinear, and soft matter physics 89, 013102 (2014).

[39] P. McKenna, D. C. Carroll, R. J. Clarke, R. G. Evans, K.W. D. Ledingham, F. Lindau, O. Lundh, T. McCanny, D. Neely, A. P. L. Robinson, L. Robson, P. T. Simpson, C.-G. Wahlstrom, and M. Zepf, *Phys. Rev. Lett*. 98, 145001 (2007).